NASA Technical Memorandum 100948
AIAA-88-3229

Experimental Vibration Damping Characteristics of the Third-Stage Rotor of a Three-Stage Transonic Axial-Flow Compressor

Frederick A. Newman
Lewis Research Center
Cleveland, Ohio

Prepared for the
24th Joint Propulsion Conference
cosponsored by the AIAA, ASME, SAE, and ASEE
Boston, Massachusetts, July 11-13, 1988

NASA

AIAA'88

AIAA-88-3229
Experimental Vibration Damping Characteristics of the Third-Stage Rotor of a Three-Stage Transonic Axial-Flow Compressor

Frederick A. Newman, NASA Lewis Research Center, Cleveland, OH

AIAA/ASME/SAE/ASEE 24th JOINT PROPULSION CONFERENCE

JULY 11-13, 1988/Boston, Massachusetts

EXPERIMENTAL VIBRATION DAMPING CHARACTERISTICS OF THE THIRD-STAGE ROTOR OF A THREE-STAGE TRANSONIC AXIAL-FLOW COMPRESSOR

Frederick A. Newman
National Aeronautics and Space Administration
Lewis Research Center
Cleveland, Ohio 44135

SUMMARY

Rotor blade aerodynamic damping is experimentally determined in a three-stage transonic axial-flow compressor having design aerodynamic performance goals of 4.5:1 pressure ratio and 65.5 lbm/sec weight flow. The combined damping associated with each mode is determined by a least squares fit of a single degree of freedom system transfer function to the nonsynchronous portion of the rotor blade strain gage output power spectra. The combined damping consists of the aerodynamic damping and the structural and mechanical damping. The aerodynamic damping varies linearly with the inlet total pressure for a given corrected speed, weight flow and pressure ratio while the structural and mechanical damping is assumed to remain constant. The combined damping is determined at three inlet total pressure levels to obtain the aerodynamic damping. The third-stage rotor blade aerodynamic damping is presented and discussed for the design equivalent speed with the stator blades reset for maximum efficiency. The compressor overall performance and experimental Campbell diagrams for the third-stage rotor blade row are also presented.

INTRODUCTION

Successful turbomachinery design requires meeting aeromechanical as well as aerodynamic performance goals. Flutter and forced response vibrations can exceed blade fatigue strengths and significantly reduce useful blade life. The prediction of flutter and forced response behavior requires knowledge of both the blade structural response and unsteady aerodynamic loading. Structural dynamics analyses (ref. 1) used to predict turbomachinery blading structural response provide useful frequency and mode shape predictions as well as the static stress levels. Current first principles unsteady aerodynamic analysis (ref. 2) allow the prediction of certain flutter modes. However, at present the amplitude of the forced response can not be predicted using unsteady aerodynamic analysis alone.

Typically forced response vibrations are predicted with a Campbell diagram which identifies the intersections of blade natural frequencies and engine order excitations. Figure 1 shows the Campbell diagram for the third-stage compressor rotor blade examined in the present investigation. Shown on the diagram are the predicted first bending, first torsion, and second bending modes of the compressor blade vibration for the range of compressor operating speeds. The diagram identifies the speed at which each blade mode coincides with engine order excitations, but does not give information about vibration levels. As can be seen in the Campbell diagram it is not usually possible to avoid all resonances in the operating range of a turbomachine. With multiple blade rows this situation is worse. The blade designer must avoid severe

resonances using mostly past experience and extensive testing of flight hardware.

At the resonances identified on the Campbell diagram, forced vibration amplitudes depend only upon the excitation and damping levels (ref. 3). Many excitations exist in multiple blade row turbomachines. Inlet distortion, wakes from upstream blade rows, potential interactions with downstream blade rows, surge, rotating stall, blade tip rubs and shaft unbalance are all potential sources of blade excitation. With appropriate aerodynamic and mechanical design, the effects of surge, rotating stall and blade tip rubs can be eliminated during normal turbomachine operation while the effects of shaft unbalance can be minimized. Some inlet distortion, wakes, and potential interactions will always exist during normal operation.

Turbomachinery blades typically have very little structural, mechanical, and other forms of nonaerodynamic damping (ref. 4). The motion of a vibrating airfoil in a moving air stream is accompanied by an unsteady lift and moment that can either damp or amplify the airfoil vibration depending upon the aerodynamic conditions. The effect of this motion dependent aerodynamics is referred to as the aerodynamic damping (refs. 5 and 6). Since the aerodynamic damping can be greater than all other forms of damping in turbomachinery blades its quantification is very important.

The unsteady aerodynamic theory associated with turbomachinery blade vibration has been developed primarily to circumvent flutter. Reference 7 provides an outline of the development of unsteady aerodynamic theory and outlines the theory. In linearized unsteady aerodynamic theory forced response is obtained from separate estimates of damping and exciting forces. The exciting or gust force is the unsteady pressure load due to passage of a gust past a rigid airfoil. The aerodynamic damping results from the motion of the airfoil in response to the unsteady gust force. The linearized unsteady aerodynamic theories used to predict flutter may also be used to predict the aerodynamic damping in the forced response problem. With the quantification of the unsteady forces and moments exciting the blade vibrations, the forced response problem can be solved for linear theory.

A survey of measurements and measurement techniques in flutter and forced response research is also presented in reference 7. The important tradeoffs between experiments in cascades and low speed rotating rigs that yield detailed data for model verification and experiments in high speed rotating rigs with realistic environments is noted. Despite the difficulty of obtaining detailed data in the high speed rotating rigs it is necessary to evaluate the unsteady aerodynamic models in realistic high speed environments.

Measurement of the aerodynamic damping in a high speed turbomachine appears in the literature. The aerodynamic damping in a high speed rotating fan was measured by Crawley (ref. 8). A flow disturbance was created upstream of the fan. When the disturbance was suddenly removed a modal analysis of the fan response yielded the aerodynamic damping.

In the present investigation the rotor blade aerodynamic damping is determined in a three-stage transonic axial-flow compressor. The damping is determined with conventional strain gages. The total damping associated with the first bending and first torsion modes is determined from rotor blade strain

gage broadband power spectra. A single degree of freedom (SDOF) transfer function is fit to each mode of interest. By repeating the measurements at three inlet total pressures and assuming only the aerodynamic damping varies with inlet pressure the aerodynamic damping is determined. The aerodynamic damping is presented for the design equivalent speed with the compressor variable geometry reset to the maximum efficiency position. The compressor overall performance and experimental Campbell diagrams for the third stage are also presented.

The determination of the aerodynamic damping for the condition presented here and at 70, 80, and 90 percent design equivalent speeds with the variable geometry at its design position is presented in reference 9. A more detailed coverage of the data reduction procedures and a simplified model of the aerodynamic damping also appears in reference 9.

SYMBOL LIST

F_d damping force, lbf

F_{da} aerodynamic damping force, lbf

F_{ds} structural and mechanical damping force, lbf

f frequency, Hz

f_n natural frequency, Hz

G_{xx} excitation autospectral density function (one sided), lbf^2/Hz

G_{yy} response autospectral density function (one sided), psi^2/Hz

H frequency response function, psi/lbf

k spring constant (expressed as force per unit stress), lbf/psi

N percent of design speed of 16 042 rpm

P stagnation pressure, psia

T stagnation temperature, °R

w compressor mass flow, lbm/sec

γ ratio of specific heats

δ ratio of compressor inlet stagnation pressure to standard pressure of 14.7 psia

ζ combined damping ratio

ζ_a aerodynamic damping ratio

ζ_s structural and mechanical damping ratio

η_{ad} adiabatic efficiency, $\dfrac{\left(P_{ex}/P_{in}\right)^{\frac{\gamma-1}{\gamma}} - 1}{\frac{T_{ex}}{T_{in}} - 1}$

θ ratio of compressor inlet stagnation pressure to standard temperature of 518.7 °R

APPARATUS AND PROCEDURE

Research Compressor

A three-stage transonic axial flow compressor was experimentally studied in the NASA Lewis Research Center Multistage Compressor Test Facility. The compressor is the first three stages of a five-stage core compressor design, designated 74B. The low aspect ratio compressor is typical of the front stages of an advanced aircraft engine core compressor. The design point aerodynamic performance goals for the first three stages are 65.5 lbm/sec mass flow, 4.5:1 total pressure ratio, and 1.4 inlet relative Mach number at rotor one leading edge tip. Blade design loss values were estimated high to favor off design performance and stage matching. This resulted in a low design efficiency of 80 percent. The compressor inlet guide vane and three stator blade rows are equipped with remotely controllable variable geometry. The aerodynamic design of compressor 74B parallels that of compressor 74A which is discussed in reference 10. The Ti-6Al-4V third-stage rotor blade is sketched in figure 2. The rotor blade base is inserted into a slot machined into the rotor wheel.

Compressor Test Facility

The NASA Lewis Multistage Compressor Test Facility is described in detail in reference 11. A schematic diagram of the facility is shown in figure 3. Briefly, atmospheric air enters the test facility through a filtered inlet located on the roof of the building and flows through a flow measuring orifice, and then through two inlet butterfly throttle valves which control the pressure in the inlet plenum tank. The air then passes through the test compressor and into the collector to be dumped to either the atmosphere or to an altitude exhaust system. Mass flow is controlled with a sleeve valve located approximately one compressor length downstream of the compressor. With the altitude exhaust system operating during this series of experiments the sleeve valve remains choked. The compressor is driven with a 15 000 hp synchronous electric motor through a 5.21:1 speed increasing gearbox.

Instrumentation

The mass flow is determined with a standard ASME sharp-edge thin-plate orifice with 1-diameter and 1/2-diameter taps. The compressor inlet total

pressure is assumed equal to the measured plenum static pressure. The compressor inlet total temperature is assumed equal to the measured plenum total temperature. Compressor exit conditions are measured with four rakes located approximately 90° apart 2.5 in. downstream of the third stage stator trailing edge. Each rake has five total-pressure-total-temperature elements located at 10, 30, 50, 70, and 90 percent of the annulus span. Static pressures at each rake element are linearly interpolated from measured inner and outer wall static pressures in the constant diameter section of the annulus. The rake measuring station is shown in figure 4. At the design equivalent speed at the maximum efficiency stator schedule, performance was measured with two of four rakes in place. The compressor rpm is determined with an electronic speed counter and magnetic pickup located above a 96 tooth gear on the drive motor shaft.

Four blades of each of the three rotor and stator blade rows are instrumented with two 350 Ω strain gages. The gages with approximately 0.0625 in. square active elements are located at or near the predicted position of maximum strain in the first bending and first torsion modes of the airfoils. Rotor blade strain gage signals are obtained from the rotating environment with a rotating data package described in reference 12. Power is delivered to the rotating data package and data is obtained from it with a rotating transformer. A switching circuit provides the output from a single gage at any time. The strain gage signals can be accessed in a sequential scanning pattern or a single gage can be monitored.

A proximity probe located to measure the orbit of the shaft connecting the compressor and gearbox provides the compressor one per rev frequency for signal analysis. Rotor strain gage signals and the one per revolution signal are recorded on FM tape for post processing. The data are post processed with a digital signal analysis system.

The estimated errors of the data based upon inherent inaccuracies of the instrumentation and recording system are as follows:

Mass flow, lbm/sec	±0.7
Temperature, °R	±1
Inlet total pressure, psi . . .	±0.2
Outlet total pressure, psi . . .	±0.6
Outlet static pressure, psi . . .	±0.6
Rotative speed, rpm	±30
Rotor blade strain, percent	±5

The aerodynamic measurements errors are taken from reference 10 for a similar test. The strain error is taken from reference 12.

Test Procedure

The compressor overall aerodynamic performance is obtained by operating the compressor at constant equivalent speed and decreasing the mass flow with the downstream throttle. Data are recorded at successive throttle positions from the maximum flow to stalled flow. Stalled flow is identified by increases in

stress levels, exit temperature and decreases in pressure ratio, weight flow, and efficiency.

The compressor variable geometry is reset at each speed to obtain maximum efficiency. The compressor is operated at the maximum efficiency throttle position with the design stator settings at each speed. The inlet guide vanes are then reset searching for the maximum efficiency position. Next with the IGVs in their maximum efficiency position the first stage stator vanes are reset searching for the maximum efficiency. Then with the IGVs and stator one in their maximum efficiency positions the second stage stator is reset searching for the maximum efficiency position. The procedure is then repeated for the third stage stator with the upstream blade rows at their maximum efficiency positions. Following resetting the third stage stator, the inlet guide vane is reset again searching for the maximum efficiency. This completes the procedure, no attempt is made to reset any of the downstream stators again.

Rotor blade strain gage data are obtained by recording the strain gage data at successive throttle positions along a constant equivalent speed line as for the overall aerodynamic performance data. Strain gage data for Campbell diagrams is recorded with the rotating data system scanning at 1.6 sec/gage. The data recorded to identify the damping is recorded for 6 min with the data system fixed on one gage. This is repeated for each gage. When obtaining strain gage data the aerodynamic performance is also obtained.

Overall Performance Data Reduction

The compressor overall aerodynamic performance is determined from the compressor inlet and exit conditions. The compressor speed and mass flow are corrected to standard day based upon compressor inlet total temperature and pressure. The total pressure ratio is determined from the mass averaged exit rake total pressure and the inlet total pressure. The adiabatic efficiency is determined assuming constant specific heats. The mass averaged isentropic temperature rise, or energy averaged total pressure ratio, is determined using the average of the specific heat ratio at the compressor inlet and exit. The compressor total temperature ratio is determined from the mass averaged exit total temperature and the inlet total temperature. Exit total temperatures are corrected for recovery variation with Mach number.

Strain Gage Data Reduction

The measured dynamic strain is proportional to the dynamic strain gage resistance changes and inversely proportional to the data system gain. The data system gain is determined prior to testing. The gain is essentially constant over the range of frequencies including the first bending modes of each of the three rotor blade rows. Using an average gain the strain is directly proportional to the data system output voltage. The rotor blade dynamic stress is calculated from the measured strain using Hooke's law and assuming the strain gage is aligned with the maximum dynamic strain.

Campbell diagrams are constructed by plotting the rotor blade response frequency against the compressor rpm. The blade response frequency is taken from the peaks in the strain gauge output power spectra. The compressor rpm is obtained from peaks in the power spectra of the one per rev signal. The

data is filtered at 5000 Hz and digitized at 12 800 samples/sec to avoid aliasing. The power spectra (ref. 13) are determined from a single squared fast Fourier transform (FFT) of 8192 data samples and have a frequency resolution of 1.56 Hz. During initial testing a twice per rev with high harmonic content was recorded instead of the once per rev. In this case the rpm is determined from the higher harmonics resulting in a greater resolution in determining the mechanical speed.

Alternating stress levels in each mode are determined from the peak positive and negative stresses in 512 sample time traces which are digitized at the same rates as above. The alternating stress is taken as one-half the difference between the peaks. This does not necessarily correspond to the stress in each mode since more than one mode may be contributing; however for the resonant stresses measured the response is primarily in a single mode.

The damping in each mode is determined by curve fitting a SDOF transfer function to the nonsynchronous portion of the strain gage power spectra in the vicinity of each mode. The data are filtered at 5000 Hz. and digitized at 12 800 samples/sec. A Hanning window with compensation for lost energy is applied to reduce truncation errors. The raw power spectra is computed from the squared FFT of 8192 data samples. The power spectra is determined from nominally 300 averaged raw power spectra. Estimates of the statistical properties of power spectrum estimates are given in reference 14. For the measurements reported herein the normalized bias and random errors inherent in the power spectral estimation are approximately .004 and .06 respectively. These errors do not limit the determination of the rotor blade combined damping and natural frequencies.

The SDOF transfer function curve fitting procedure is developed as follows. The frequency response function is defined as (refs. 13 and 14)

$$H(f) = \frac{Y(f)}{X(f)} \tag{1}$$

where $X(f)$ and $Y(f)$ are the Fourier transforms of the input and output respectively. Squaring this gives

$$|H(f)|^2 = \frac{G_{yy}(f)}{G_{xx}(f)} \tag{2}$$

where $G_{xx}(f)$ and $G_{yy}(f)$ are the input and output power spectrum respectively. Assuming the input spectrum is Gaussian or white noise the input power spectrum is constant. Writing the frequency response function or transfer function for a SDOF system with viscous damping gives

$$\frac{G_{yy}(f)}{G_{xx}} = \frac{1/k^2}{(1 - (f/f_n)^2)^2 + (2\zeta\, f/f_n)^2} \tag{3}$$

which can be written as

$$\frac{k^2}{G_{xx}} - \left(2 - 4\zeta^2\right) \frac{k^2}{G_{xx} f_n^2} f^2 + \frac{k^2}{G_{xx} f_n^4} f^4 = \frac{1}{G_{yy}(f)} \tag{4}$$

or

$$C_1 + C_2 x + C_3 x^2 = y \tag{5}$$

The undamped natural frequency, combined damping ratio and the constant, k^2/G_{xx}, are determined from a least square fit (ref. 15) of equation 5 to the nonsynchronous peak in the data for each mode of interest.

The aerodynamic damping is determined from combined damping measurements at three inlet total pressures for each operating point. The measured combined damping consists of structural, mechanical, and aerodynamic damping. The aerodynamic damping is the result of the unsteady aerodynamic loading on the airfoil and can be normalized with the dynamic pressure of the flow. Neglecting Reynolds number and heat transfer effects, the dynamic pressure at any point in the compressor depends only on the inlet total pressure for a given equivalent speed, equivalent mass flow and pressure ratio.

Assuming the structural and mechanical damping does not vary with inlet pressure at a given operating point the damping force on the rotor blade can be written

$$F_d = F_{ds} + F_{da,std} \left(\frac{P}{P_{std}}\right)$$

With the damping force proportional to the damping ratio we have

$$\zeta = \zeta_s + \zeta_{a,std} \left(\frac{P}{P_{std}}\right) \tag{6}$$

The aerodynamic damping ratio at the standard day inlet pressure is the slope of the combined damping ratio-inlet total pressure relation.

RESULTS AND DISCUSSION

The overall aerodynamic performance of the three-stage transonic axial compressor with the inlet guide vanes and stators at their design setting angles is shown in figure 5. The overall performance data were acquired at a nominal compressor inlet total pressure of one-half atmosphere. The compressor total pressure ratio and adiabatic efficiency are plotted against equivalent mass flow for 50, 70, 80, 90, and design corrected speed. The compressor mass flow exceeds the design flow at the design speed. The excess in flow rate is comparable to that of a similar compressor, designated 74A, reported in reference 10.

The compressor overall performance with the inlet guide vanes and stators reset for maximum efficiency at each speed is presented in figure 6. Again the overall performance data were acquired with the compressor inlet total pressure nominally one-half atmosphere. Table 1 lists the vane reset schedule at each speed and figure 7 defines the vane reset direction. The flow exceeds

its design value as it did prior to resetting the vanes. No attempt was made to obtain the design flow while resetting the vanes. The efficiency at the design speed increased nearly 6 points from that with the vanes at their design positions. A low design efficiency had been selected to benefit part speed performance and matching. The increase in efficiency at the design speed is consistent with the performance of compressor 74A in reference 10.

Campbell diagrams and stress level plots for the third stage rotor blade row are presented in figures 8-10. The first bending and first torsion modes measured on the same blade are shown in each diagram. The response in each mode is identified with the gage positioned to measure the maximum response in that mode. The open symbols are the measured response frequencies of the highest stress in each mode at each mechanical speed shown. The solid lines are the blade natural frequencies predicted by finite element analysis. Also shown are the measured stress levels. For convenience, only stresses in the indicated modes above 500 psi are shown. The three figures correspond to the three third-stage rotor blades for which the aerodynamic damping is presented. The strain gage numbers are noted on the figures. Data was not obtained and is not shown in the first bending mode below 11 710 rpm for gage 24 in figure 10.

The data shown in the Campbell diagrams are acquired with the compressor throttle in its full open position and the variable stators set at the design positions. The data at the full open position are shown so the effects of stall at low speeds does not complicate the data.

The predicted frequency response describes the trends in the first bending mode. The forced response vibrations are excited by unsteady flows at the engine order frequencies. The measured frequencies do not trace out the mode frequency variation with speed since the excitations do not coincide with the natural frequency at all operating speeds. The highest stresses occur at resonance where the engine order and natural frequencies coincide. High stresses are predicted at 11 710 rpm in figures 8 and 10 and at 14 060 rpm in figure 10. At several other operating points the high stresses are not coincident with the predicted frequency speed relation.

The greatest stress in the first bending mode occurs at 11 710 rpm at 7 per rev. The stress level shown is 6000 psi. The compressor has 32 second stage rotor blades and 39 third stage rotor blades. The difference in the number of these rotor blades causes an unsteady flow for the second stage stator row due to the wakes convected downstream from the second stage rotors and the upstream potential influence of the third stage rotor blades. The third stage rotor blades moving through the unsteady wake pattern from the second stage stator row experience this 7 per rev excitation.

The data in the first torsion mode is not described by the predicted frequency curve. The torsion frequency decreases with compressor rpm for each of the three blades shown. This decrease may be due to increased flexibility of the rotor wheels with speed or a decrease in stiffness of the blades due to temperature. There are no significant stresses measured in torsion on the third stage rotor blades.

The averaged output power spectra for the third-stage rotor blade instrumented with gage number 19 at the design equivalent speed is shown in figure 11(a). The data was acquired with the stator blades set to the maximum efficiency schedule with the inlet pressure at one-half atmosphere at the

throttle position identified in figure 6. Figure 11(a) shows both engine order response and nonsynchronous responses. The engine order responses are periodic and are seen as spikes at all multiples of the rotational speed. The nonsynchronous response outlines the first bending, first torsion, and second bending modes of the rotor blade. Figure 11(b) highlights the first torsion mode in figure 11(a) and the SDOF transfer function fit to the data. The curve fit was performed to the data near the nonsynchronous peak between 3103 and 3165 Hz. The curve fit follows the data beyond the frequency range to which it was fit. The SDOF transfer function describes the individual modes and establishes the undamped natural frequency and combined damping ratio.

The aerodynamic damping ratio at the standard day inlet pressure is given by equation (6) as the slope of the measured damping ratio variation with inlet total pressure. Figure 12 is the variation of the measured damping ratio with inlet total pressure for the third stage rotor blade first bending mode at design equivalent speed. The data was obtained with the variable vanes reset to the maximum efficiency positions and the throttle 80 percent open. The compressor overall performance at this position is identified on figure 6. The measured damping ratios follow the linear relation. Also shown on figure 12 is a least squares approximation to equation (6)

$$\zeta = 0.00134 + 0.0120\ P_{in}/P_{std}$$

The aerodynamic damping is the greatest portion of the measured damping even at the lowest of the three inlet pressures.

The variation of the measured damping in the first torsion mode for the same operating conditions as figure 12 is shown in figure 13. Also shown is the least squares approximation of equation (6) through the data.

$$\zeta = -0.000326 + 0.00994\ P_{in}/P_{std}$$

The least squares fit through all the data results in a small negative nonaerodynamic damping. The structural and mechanical damping in the first torsion mode is anticipated to be small (ref. 4). The difference between the negative value determined and the actual nonaerodynamic damping is realistically within the accuracy of the data.

Determination of the aerodynamic damping in a realistic high speed environment allows assessing unsteady aerodynamics models. Predictions of forced response during the design phase of new generation turbomachines will greatly enhance the designers ability to deviate from past experience. Determination of the aerodynamic damping also allows assessing forced response of a proven compressor in different applications. High Mach number applications are of particular interest. High inlet pressures associated with high flight speed may encourage additional forced response problems. This is true also of a compressor operating behind a new high pressure ratio fan. So long as the Reynolds number change does not significantly effect the flows forcing the vibrations the alternating stress can be assessed knowing the damping variation with inlet pressure.

SUMMARY OF RESULTS

The aerodynamic damping is determined from rotor blade strain gage output power spectra. A SDOF transfer function is fit to the peak of the power spectra in each mode. The transfer function describes the data and provides the damping and natural frequency. By assuming the structural and mechanical damping do not vary with inlet pressure the aerodynamic damping is determined at constant equivalent speed. Damping measurements at three inlet total pressures provide the aerodynamic and the structural and mechanical damping.

The aerodynamic damping is determined for the third stage rotor blade at the design equivalent speed in the first bending and first torsion modes. The aerodynamic component is the greatest portion of the combined damping at all the inlet pressures tested in both bending and torsion.

REFERENCES

1. Kielb, R.E., Leissa, A.W., and Macbain, J.C., "Vibrations of Twisted Cantilever Plates - A Comparison of Theoretical Results," International Journal for Numerical Methods in Engineering, Vol. 21, No. 8, 1985, pp. 1365-1380.

2. Whitehead, D.S., "Force and Moment Coefficients for Vibrating Airfoils in Cascade," British A.R.C. R&M-3254, Feb. 1960.

3. Thomson, W.T., Vibration Theory and Applications, Third Edition, Prentice-Hall Inc., Englewood Cliffs, NJ, 1965.

4. Srinivasan, A.V., Cutts, D.G., and Sridhar, S., "Turbojet Engine Blade Damping," REPT-R81-91441031, United Technologies Research Center, East Hartford, CT, July 1981, NASA CR-165406.

5. Bisplinghoff, R.L., Ashley, H., and Halfman, R.L., Aeroelasticity, Addison-Wesley Publishing Co. Inc., Cambridge, MA, 1955.

6. Carta, F.O., "Aeroelasticity and Unsteady Aerodynamics," The Aerothermodynamics of Aircraft Gas Turbine Engines, G.C. Oates, ed., AFAPL-TR-78-52, 1978, Chapter 22. (Avail. NTIS, AD-A059784.)

7. Platzer, M.F., and Carta, F.O., eds. Aeroelasticity in Axial-Flow Turbomachines, Vol. 1 - Unsteady Turbomachinery Aerodynamics, AGARD-AG-298-VOL-1, AGARD, Neuilly-Sur-Seine, France, 1987. (Avail. NTIS, AD-A181676.)

8. Crawley, E.F., "Measurements of Aerodynamic Damping in the MIT Transonic Rotor," GTL-157, Massachusetts Institute of Technology, Cambridge, MA, Feb. 1981, NASA CR-163988.

9. Newman, F.A., "Experimental Determination of Aerodynamic Damping in a Three-Stage Transonic Axial-Flow Compressor," NASA TM-100953, 1988.

10. Steinke, R.J., "Design of 9.271-Pressure-Ratio Five-Stage Core Compressor and Overall Performance for First Three Stages," NASA TP-2597, 1986.

11. Cunnan, W.S., Stevens, W., and Urasek, D.C., "Design and Performance of a 427-Meter-per-Second Tip-Speed Two-Stage Fan Having a 2.40 Pressure Ratio," NASA TP-1314, 1978.

12. Lesco, D.J., Sturman, J.C., and Nieberding, W.C., "On-The-Shaft-Date Systems for Rotating Engine Components," NASA TM X-68112, 1972.

13. Bendat, J.S., and Piersol, A.G., Random Data: Analysis and Measurement Procedures, Wiley-Interscience, New York, 1971.

14. Bendat, J.S., and Piersol, A.G., Engineering Applications of Correlation and Spectral Analysis, Wiley-Interscience, New York, 1980.

15. James, M.L., Smith, G.M., and Wolford, J.C., Applied Numerical Methods for Digital Computation with Fortran and CSMP, Second Edition, Harper & Row, New York, 1977.

TABLE I. - MAXIMUM EFFICIENCY IGV-STATOR SETTING ANGLES

Percent design speed	Reset (degrees)			
	IGV	Stator 1	Stator 2	Stator 3
50	29	10	2	-8
70	21	10	0	-8
80	18	10	0	0
90	15	6	2	0
100	0	10	6	10

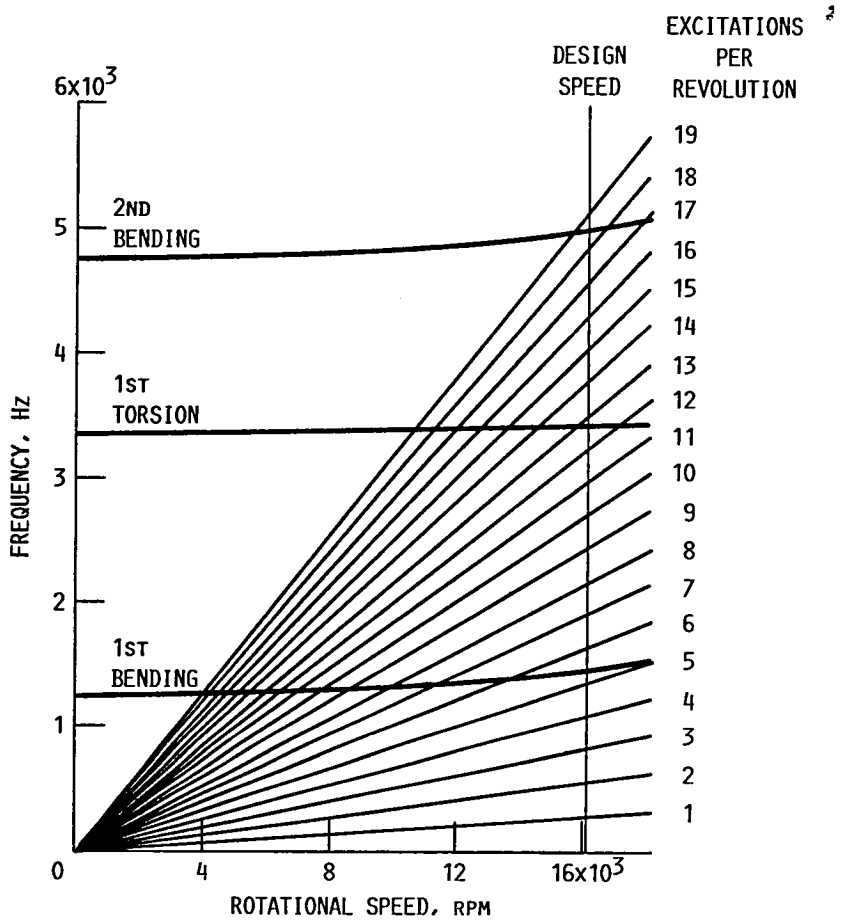

FIGURE 1. - THIRD-STAGE ROTOR BLADE CAMPBELL DIAGRAM.

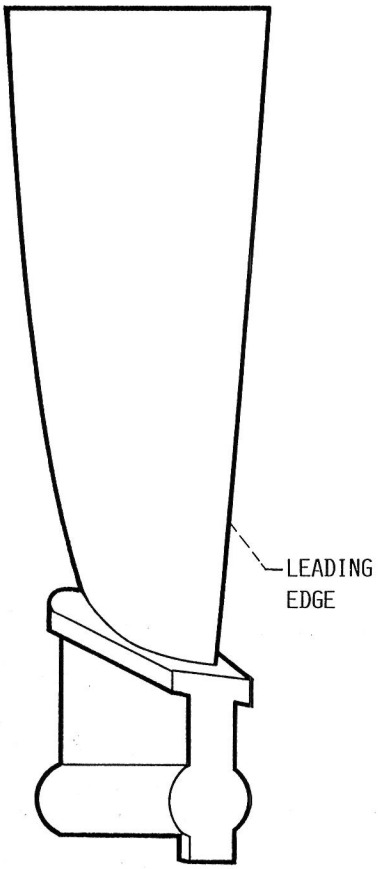

FIGURE 2. - COMPRESSOR ROTOR BLADE LOOKING DOWNSTREAM ALONG AXIS OF ROTATION. NOT TO SCALE.

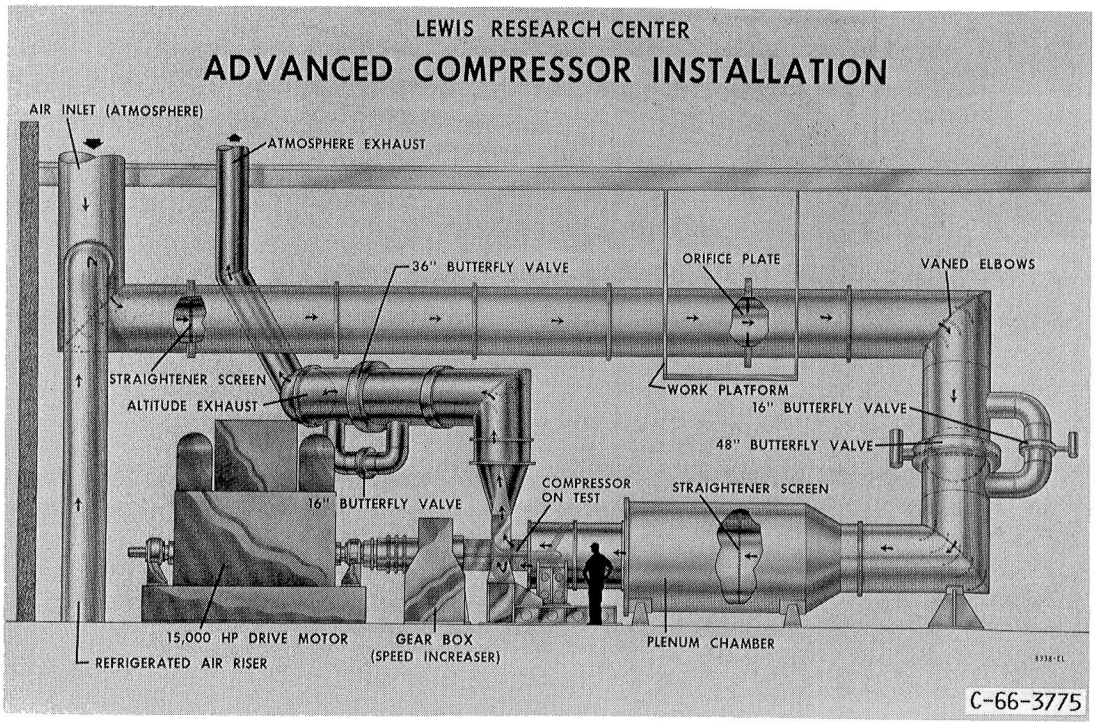

FIGURE 3. - MULTISTAGE COMPRESSOR TEST FACILITY.

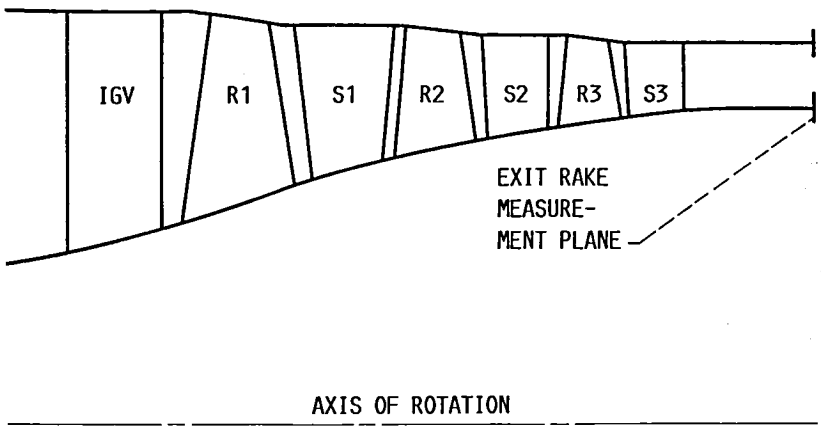

FIGURE 4. - FLOWPATH FOR FIRST THREE STAGES OF COMPRESSOR 74B.

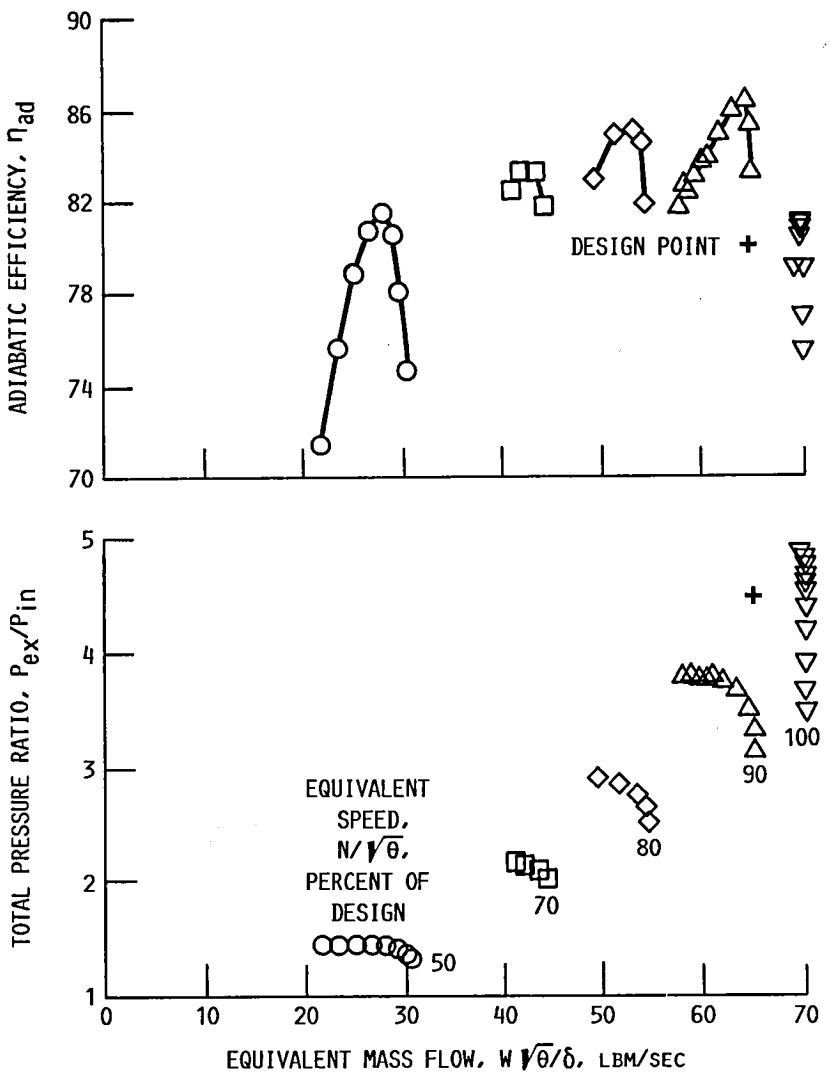

FIGURE 5. - PERFORMANCE OF FIRST THREE STAGES OF COMPRESSOR 74B AT DESIGN IGV-STATOR SETTING ANGLES.

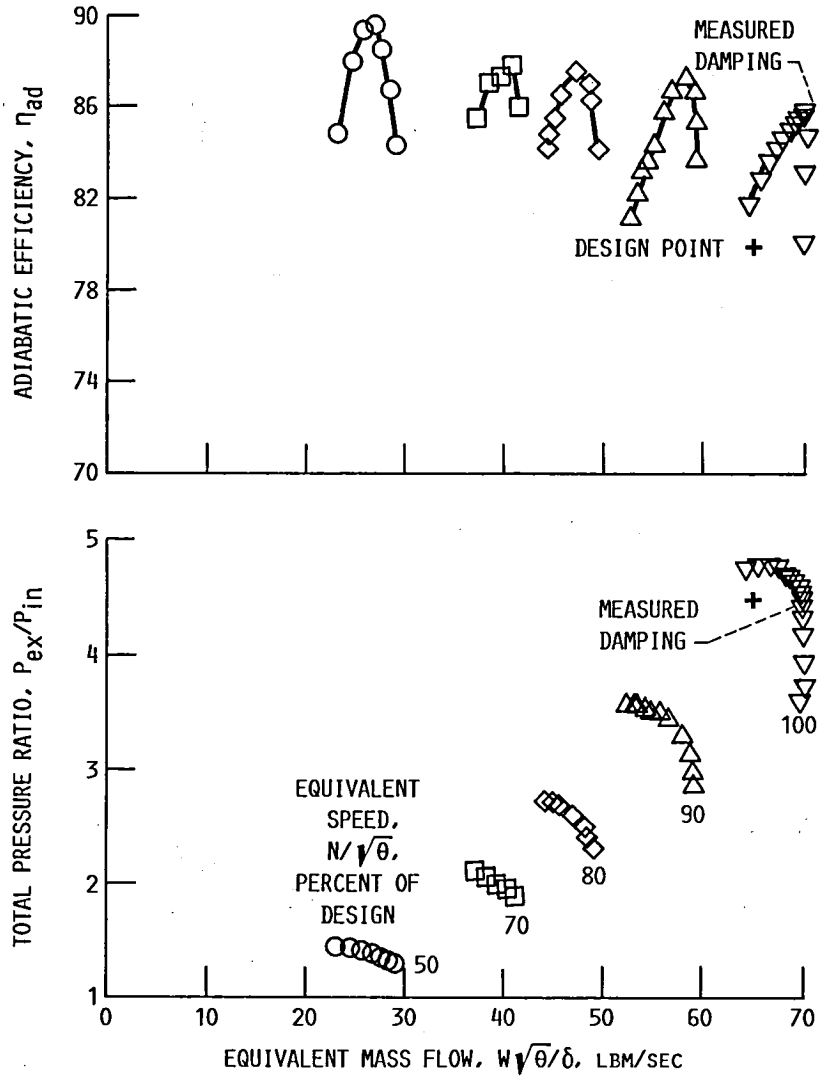

FIGURE 6. - PERFORMANCE OF FIRST THREE STAGES OF COMPRESSOR 74B AT MAXIMUM EFFICIENCY IGV-STATOR SETTING ANGLES AT EACH SPEED SHOWN.

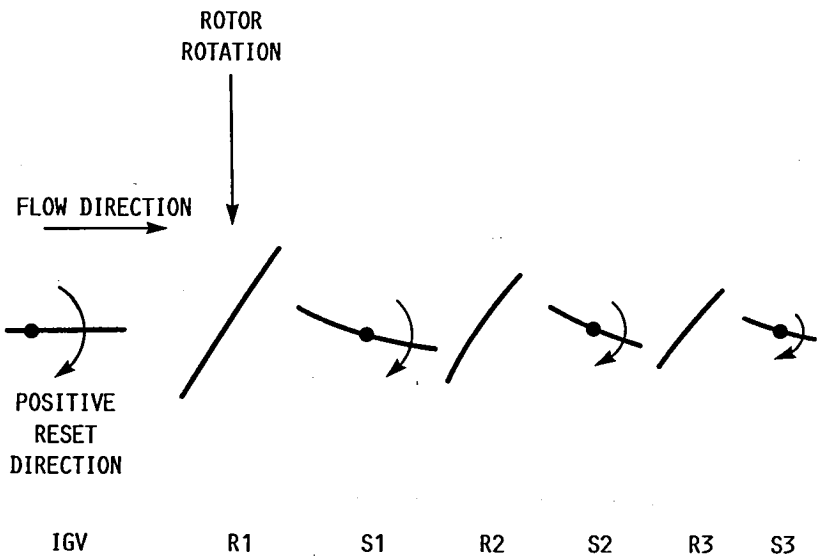

FIGURE 7. - SCHEMATIC OF BLADE ROWS WITH POSITIVE DIRECTION OF VANE RESET SPECIFIED.

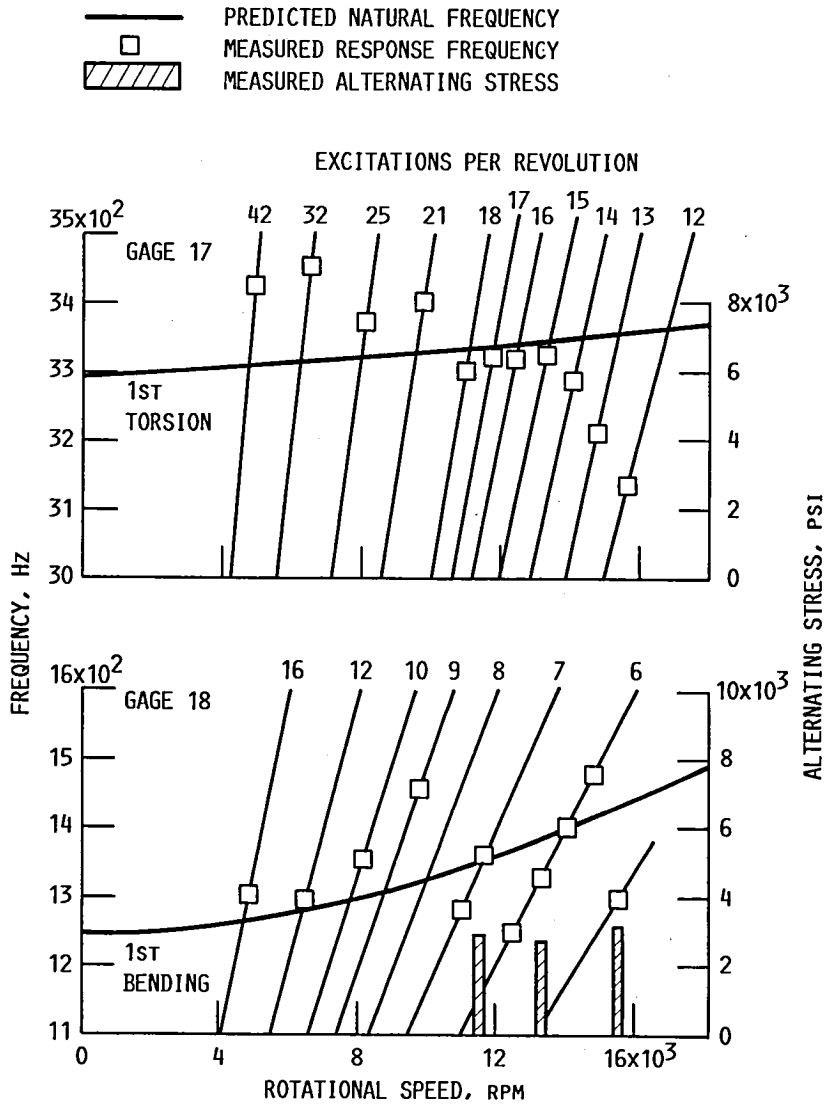

FIGURE 8. - EXPERIMENTAL CAMPBELL DIAGRAM WITH ALTERNATING STARESS LEVELS FOR THIRD-STAGE ROTOR BLADE INSTRUMENTED WITH GAGES 17 AND 18. (ONLY MEASURED STRESSES ABOVE 500 PSI SHOWN.)

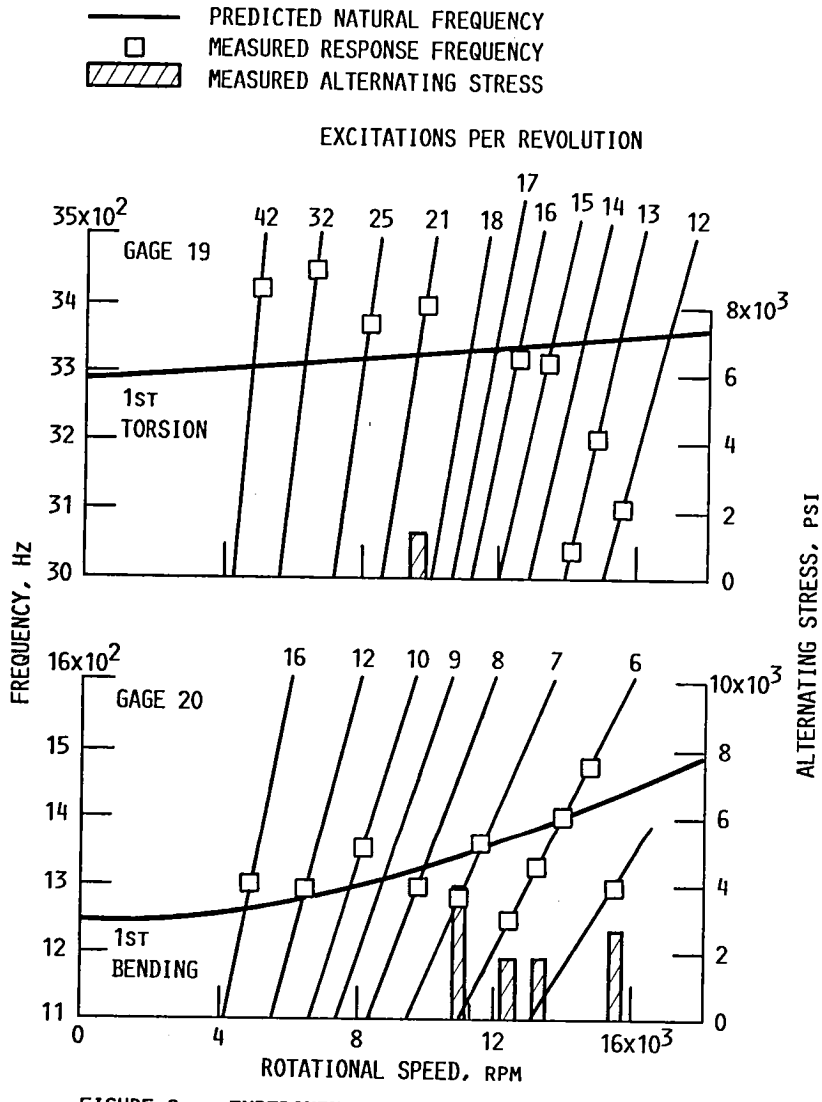

FIGURE 9. - EXPERIMENTAL CAMPBELL DIAGARAM WITH ALTERNATING STRESS LEVELS FOR THIRD-STAGE ROTOR BLADE INSTRUMENTED WITH GAGES 19 AND 20. (ONLY MEASURED STRESSES ABOVE 500 PSI SHOWN.)

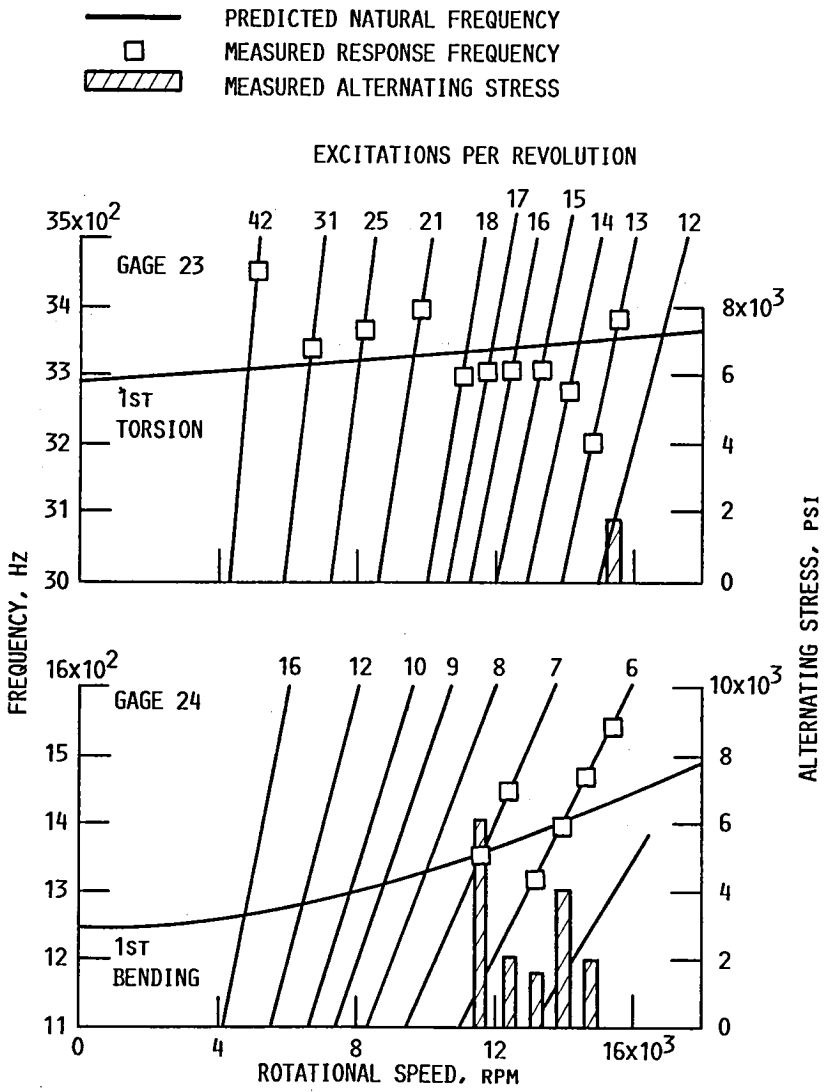

FIGURE 10. - EXPERIMENTAL CAMPBELL DIAGRAM WITH ALTERNATING STRESS LEVELS FOR THIRD-STAGE ROTOR BLADE INSTRUMENTED WITH GAGES 23 AND 24. (ONLY MEASURED STRESSES ABOVE 500 PSI SHOWN.)

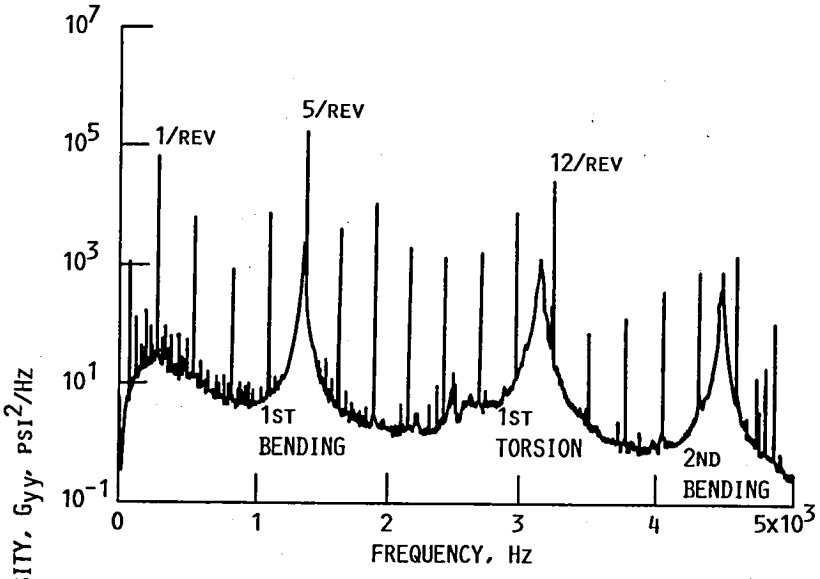

(a) FULL DATA BANDWIDTH.

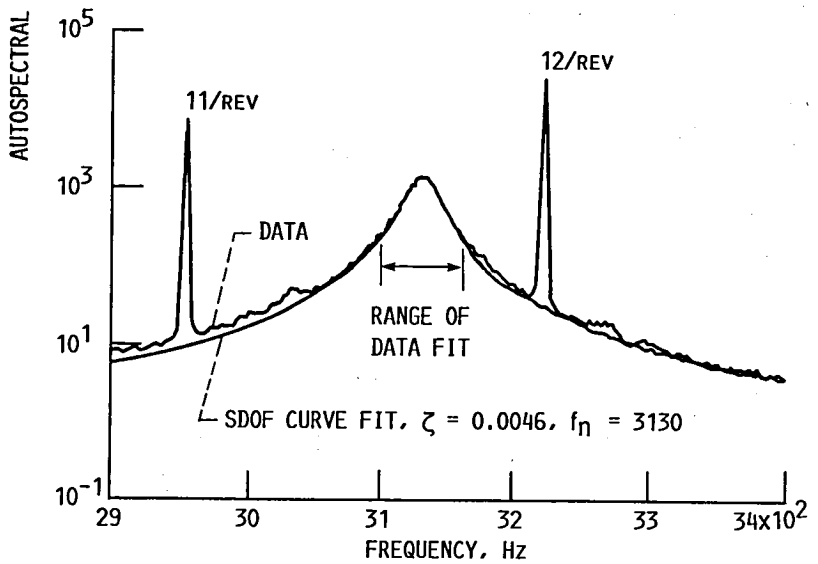

(b) 1ST TORSION MODE AND SDOF CURVE FIT.

FIGURE 11. - ROTOR THREE STRAIN GAGE 19 OUTPUT POWER SPECTRA AT DESIGN EQUIVALENT SPEED WITH IGV-STATOR SETTING ANGLES AT MAXIMUM EFFICIENCY POSITIONS AND 1/2 ATM INLET TOTAL PRESSURE.

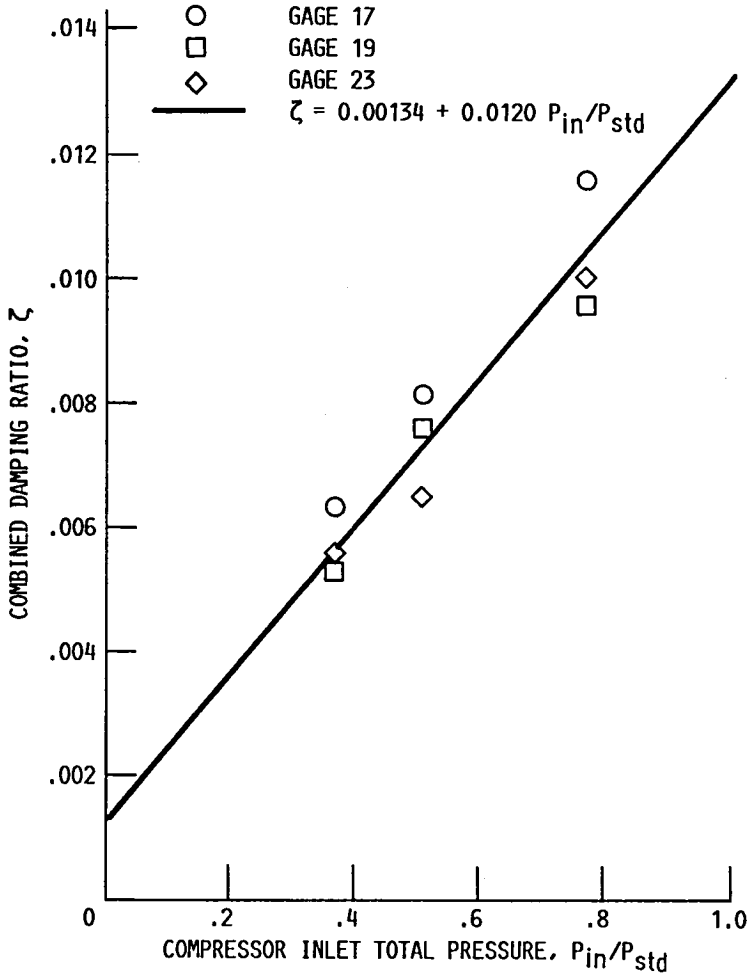

FIGURE 12. - ROTOR THREE FIRST BENDING MODE COMBINED DAMPING RATIO VARIATION WITH INLET TOTAL PRESSURE AT DESIGN EQUIVALENT SPEED WITH IGV-STATOR SETTING ANGLES AT MAXIMUM EFFICIENCY POSITIONS.

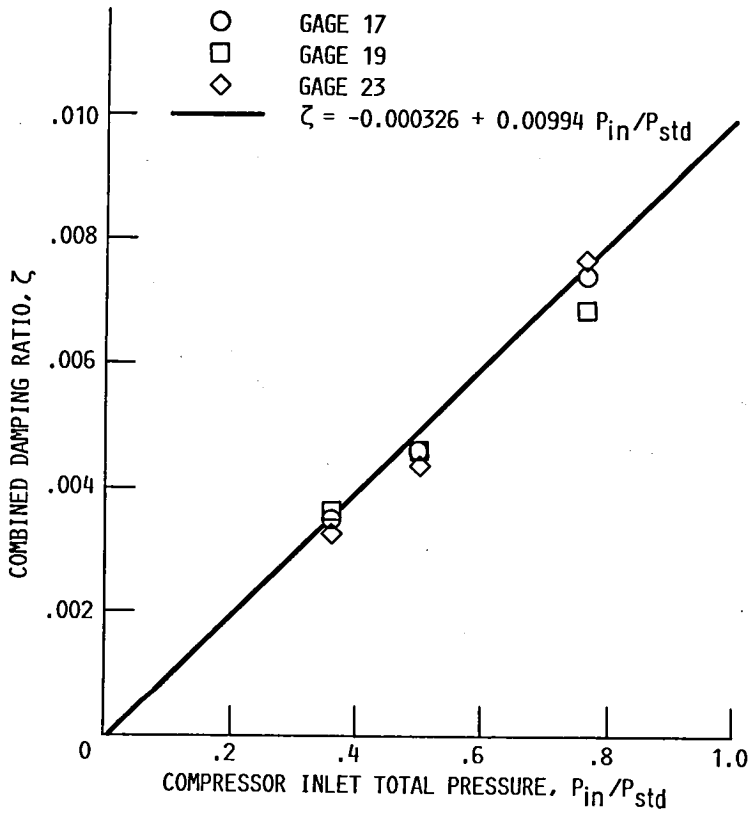

FIGURE 13. - ROTOR THREE FIRST TORSION MODE COMBINED DAMPING RATIO VARIATION WITH INLET TOTAL PRESSURE AT DESIGN EQUIVALENT SPEED WITH IGV-STATOR SETTING ANGLES AT MAXIMUM EFFICIENCY POSITIONS.

NASA
National Aeronautics and Space Administration

Report Documentation Page

1. Report No.	2. Government Accession No.	3. Recipient's Catalog No.
NASA TM-100948 AIAA-88-3229		

4. Title and Subtitle
Experimental Vibration Damping Characteristics of the Third-Stage Rotor of a Three-Stage Transonic Axial-Flow Compressor

5. Report Date

6. Performing Organization Code

7. Author(s)
Frederick A. Newman

8. Performing Organization Report No.
E-4240

10. Work Unit No.
535-05-01

9. Performing Organization Name and Address
National Aeronautics and Space Administration
Lewis Research Center
Cleveland, Ohio 44135-3191

11. Contract or Grant No.

13. Type of Report and Period Covered
Technical Memorandum

12. Sponsoring Agency Name and Address
National Aeronautics and Space Administration
Washington, D.C. 20546-0001

14. Sponsoring Agency Code

15. Supplementary Notes
Prepared for the 24th Joint Propulsion Conference cosponsored by the AIAA, ASME, SAE, and ASEE, Boston, Massachusetts, July 11-13, 1988.

16. Abstract

Rotor blade aerodynamic damping is experimentally determined in a three-stage transonic axial flow compressor having design aerodynamic performance goals of 4.5:1 pressure ratio and 65.5 lbm/sec weight flow. The combined damping associated with each mode is determined by a least squares fit of a single degree of freedom system transfer function to the nonsynchronous portion of the rotor blade strain gage output power spectra. The combined damping consists of the aerodynamic damping and the structural and mechanical damping. The aerodynamic damping varies linearly with the inlet total pressure for a given corrected speed, weight flow and pressure ratio while the structural and mechanical damping is assumed to remain constant. The combined damping is determined at three inlet total pressure levels to obtain the aerodynamic damping. The third-stage rotor blade aerodynamic damping is presented and discussed for the design equivalent speed with the stator blades reset for maximum efficiency. The compressor overall performance and experimental Campbell diagrams for the third-stage rotor blade row are also presented.

17. Key Words (Suggested by Author(s))	18. Distribution Statement
Compressor Aerodynamic damping Rotor blade vibration	Unclassified - Unlimited Subject Category 07

19. Security Classif. (of this report)	20. Security Classif. (of this page)	21. No of pages	22. Price*
Unclassified	Unclassified	24	A02

NASA FORM 1626 OCT 86

*For sale by the National Technical Information Service, Springfield, Virginia 22161

National Aeronautics and
Space Administration

Lewis Research Center
Cleveland, Ohio 44135

FOURTH CLASS MAIL

ADDRESS CORRECTION REQUESTED

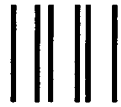

Official Business
Penalty for Private Use $300

Postage and Fees Paid
National Aeronautics and
Space Administration
NASA 451

NASA